Hindawi Publishing Corporation
Journal of Control Science and Engineering
Volume 2016, Article ID 2352805, 12 pages
http://dx.doi.org/10.1155/2016/2352805

Research Article

A Novel Relative Navigation Control Strategy Based on Relation Space Method for Autonomous Underground Articulated Vehicles

Fengqian Dou, Yu Meng, Li Liu, and Qing Gu

University of Science and Technology Beijing, Beijing, China

Correspondence should be addressed to Yu Meng; myu@ustb.edu.cn

Received 4 May 2016; Revised 7 August 2016; Accepted 6 September 2016

Academic Editor: Roberto Sabatini

This paper proposes a novel relative navigation control strategy based on the relation space method (RSM) for articulated underground trackless vehicles. In the RSM, a self-organizing, competitive neural network is used to identify the space around the vehicle, and the spatial geometric relationships of the identified space are used to determine the vehicle's optimal driving direction. For driving control, the trajectories of the articulated vehicles are analyzed, and data-based steering and speed control modules are developed to reduce modeling complexity. Simulation shows that the proposed RSM can choose the correct directions for articulated vehicles in different tunnels. The effectiveness and feasibility of the resulting novel relative navigation control strategy are validated through experiments.

1. Introduction

Underground mining has an important role in the acquisition of many of the world's natural resources, and articulated vehicles are typically used for underground mining operations, since they have the small turning radii required for navigating the narrow tunnels in most underground environments. With the application of new equipment and technology, intelligent underground mining vehicles have been the object of significant development in recent decades, which has greatly improved mining safety and efficiency [1]. Autonomous navigation is central to the operation of such vehicles, and many navigation techniques are in use, including global positioning (GPS), inertial navigation (INS), and ultrasonic positioning systems [2–4]. Many existing autonomous robots use computer vision and other sensors to supplement GPS data when navigating. However, most of these navigation methods cannot be applied in the underground due to the inherent uncertainty in the environment. For instance, there are no detectable GPS signals in underground environments, the detection range of normal ultrasonic radar is limited and unstable underground, and the cost of an INS is too high. Compared to the above-mentioned three positioning methods, laser radar is an ideal positioning device in underground environments owing to its wide detection range and reasonable cost; laser range finders have been successfully used in agricultural robots [5], for example.

Navigation methods can be divided into absolute and relative navigation according to whether the environmental model (e.g., map information) is needed or not [6]. For absolute navigation, the driving path for the vehicle must be planned beforehand. Optimal path planning and integrated local trajectory planning have been used for autonomous ground vehicles [7–9]. The vehicles' absolute position with respect to some fixed real-world coordinate system must be known (known as localization), which is normally obtained by dead reckoning through the data transferred by sensors installed in the vehicle [10–12]. This type of navigation should keep the vehicle following the predetermined path, which requires map path and artificial marking equipment. However, the cost of the positioning device in a large-scale mining operation is extremely high, and underground mining environments change with the depth of the mine, which requires the planned path to be updated in real time. Therefore, the

utilization of absolute navigation is restricted to some extent in underground mining operations.

Relative navigation, on the other hand, does not require an environmental model, and it is unnecessary to plan the driving path using an accurate position on the map. By applying the relative navigation method, the vehicle can sense its surrounding via on-board sensors that detect the shape and size of the tunnel in front of the vehicle in order to avoid collisions; the method has been widely applied by some mining companies by implementing supersonic detectors [13–15]. Traditional relative navigation has limitations in complex tunnel environments, such as the inability to choose the correct way to proceed at intersections. Therefore, Roberts has proposed a "nodal map" method to enable the relative navigation method to choose the correct way to proceed intersections [16]. However, improving the navigation driving efficiency remains a problem. In this paper, a novel relative navigation control strategy that considers the structural and driving features of articulated vehicles is proposed to improve autonomous driving efficiency. The kinematics model is built based on the articulated structure, and the steering and speed control models are built based on the vehicle's operation data, which has both high applicability and low complexity. The space information is processed using a self-organizing, competitive neural network, through which the space is divided into free space and trap space. According to the different impacts of the space information in front of the vehicle, the relation space method (RSM) is proposed as the key to a vehicle being able to choose the correct driving direction.

The remainder of this paper is organized as follows. In Section 2, we describe how to identify the space information using a self-organizing, competitive neural network and how to find the optimal strategy direction using the RSM. In Section 3, we outline the kinematics and dynamic models of an articulated vehicle. The dynamic model is built based on the data that are collected from the prototype. The control method is also described in this section. In Section 4, we focus on the results of simulation and experiment; we present conclusions in Section 5.

2. Relation Space Method

In underground mining operations, tunnel environments change over the course of tunnel length. Since there is no planned path for the vehicle using relative navigation, the information about the space around the vehicle therefore becomes very important, which not only affects the vehicle's driving mode but also determines navigational accuracy. The vehicle's navigation is designed based on the space information, and thus the navigational method proposed in this paper is designated as the relation space method. The first step in the RSM is to identify the space around the vehicle using a self-organizing, competitive neural network, which can be used to determine the vehicle's optimal driving direction based on the existing spatial geometric relationships.

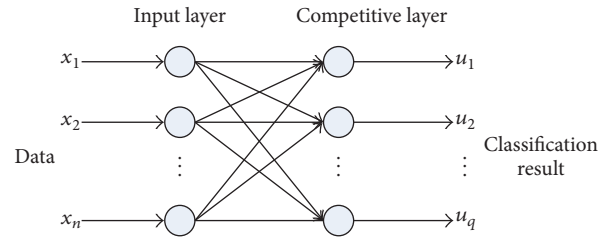

Figure 1: General structure of self-organizing, competitive neural network.

2.1. Space Identification. As mentioned above, the first step in the RSM is to identify the space. Since artificial neural networks have been widely used in statistical classification problems owing to their strong self-organizing characteristics, adaptability, fault tolerance, and reasoning ability, they have given good results [17, 18]. Thus, in this paper, we apply a self-organizing, competitive neural network to identify the space information, which is a way of training the network's self-organizing feature. In this paper, laser radar is used to detect the underground environment, leveraging its features of high resolution, strong antijamming ability, small volume, and low cost.

Figure 1 shows the basic self-organizing, competitive network structure, which includes input and competitive layers. The input sample of the network is $\mathbf{X} = [x_1, x_2, \ldots, x_n]$ and the output is $\mathbf{U} = [u_1, u_2, \ldots, u_q]$. w_{ij} denotes the competitive weight from input nodes to neurons, and it can be modified through training. The neurons in the input layer of the self-organizing network are connected to neurons in the output layer through the weight, and the neurons in the competitive layer compete with each other, and only one or a few neurons can "win" to adapt to the current input sample. The competitive learning rule is the main factor. The connection-weight value of the network is w_{ij} $(i = 1, 2, \ldots, N,\ j = 1, 2, \ldots, M)$, and it satisfies the constraint conditions

$$\sum_{i=1}^{N} w_{ij} = 1. \tag{1}$$

The input samples are binary vectors, and, for the state of competitive-layer neurons j, the weight sum of the input node is given according to (2) as follows:

$$S_i = \sum_{i=1}^{n} w_{ij} \cdot x_i. \tag{2}$$

x_i in (2) are the ith elements of the input sample vector. According to the mechanism of competition, k neurons with maximum weight values win. The output is

$$u_k = \begin{cases} 1, & S_k > S_j,\ \forall j, k \neq j, \\ 0, & \text{others.} \end{cases} \tag{3}$$

For each i, the weights after the competition are amended in accordance with

$$w_{ij} = w_{ij} + \eta \cdot \left(x_i - w_{ij}\right), \tag{4}$$

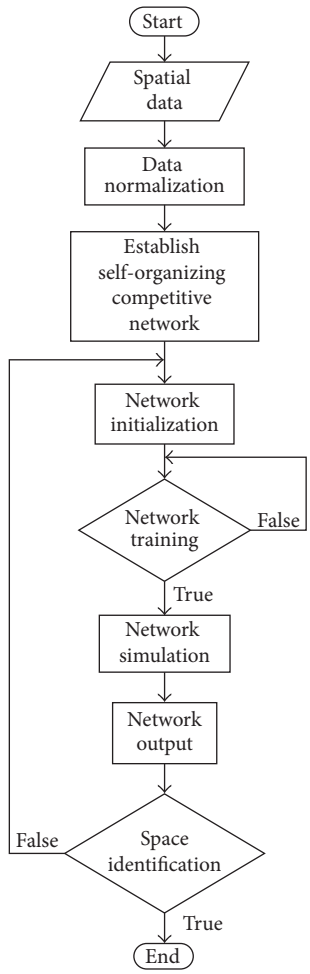

Figure 2: Flowchart of space identification process.

where η is the learning parameter, which is generally taken to be in the range of 0 to 1. In consideration of the learning efficiency, in this paper, η is set to 0.1.

Figure 2 is a flowchart of the space identification using a self-organizing, competitive neural network. The first step is to obtain the space data, collected from the laser radar, which were normalized using a normalized formula. The second step is to create the neural network, which needs to be initialized and trained. The competitive neural network is applied in no-teacher learning, and there is no desired output, so there is no need to set up the training process to judge whether the end of network training results in an error. The network training number must be set to determine the training efficiency; in this paper, it is set to 1000. After training, a simulation function is used to check the network-classified space model. If the space identification is not successful, the network should be reinitialized, retrained, and retested. There are two output types, denoted as free space and trap space. Free space is the region that the vehicle can go through and trap space is the region that the vehicle should avoid.

2.2. Optimal Driving Direction. After the space is divided into free space and trap space using the self-organizing, competitive neural network, the vehicle's optimal driving direction is determined based on the spatial geometric relationships. Figure 3 shows the free space and trap space for the vehicle in the tunnel environment, as well as an obstacle in front of the vehicle. Figure 3(a) shows all of the free and trap spaces identified using the neural network; the points marked with asterisks represent the free space and those marked with open circles represent the trap space. Figure 3(b) shows the coordinate system built for the navigational method proposed in this paper. Its origin point is located at the center of the laser radar, its y-axis is in the direction of the course angle of the vehicle, and its x-axis can be obtained by applying the right-hand screw rule. $P_i(x_i, y_i)$ are the detected points in steps of $\Delta\theta$, and $\Delta\theta = 1^\circ$ in this paper; i $(i = 1, 2, \ldots, N)$ is the index of the detected points and D_{OP_i} is the distance between the origin point O and P_i. It is known that $P_i(x_i, y_i)$ are the positions of the wall or the obstacles. In the complex environment, the free space is not unique, which is defined as the sub-free space (SFS), based on whether the index of the detected points, I, is continuous. The SFS is denoted as SF_j $(j \in Z,\ j = 1, 2, \ldots, M)$. There are two SFSs depicted in Figure 3(b), and therefore $M = 2$.

All of the SFSs are candidate driving regions, but the best direction for the vehicle still needs to be determined. The optimal strategic direction is defined as the angular bisector of two laser beams in the largest-area SFS. In order to calculate the area of the subspaces, the area formula of a triangle can be applied. The area of the two laser beams is denoted as Δ, which can be approximately calculated by

$$\Delta = \frac{1}{2} \cdot D_{OP_i} \cdot D_{OP_{i+1}} \cdot \sin(\Delta\theta). \tag{5}$$

In Figure 3, the triangles $P_O P_a P_b$ and $P_O P_c P_d$ are two SFSs, θ_j refers to the detection angle of SF_j, and the straight lines OB_j form the angular bisector of θ_j. Each OB_j is a candidate optimal strategic direction. The area of SF_j is denoted as $\Delta\mathrm{SF}_j$, and the indexes of the detected points in the two boundary beams of SF_j are denoted as U_j and V_j, respectively. On the basis of (5), $\Delta\mathrm{SF}_j$ can be calculated approximately by

$$\Delta\mathrm{SF}_j = \frac{1}{2} \cdot \sum_{k=U_j}^{V_j - 1} \left(D_{OP_k} \cdot D_{OP_{k+1}} \right) \cdot \sin(\Delta\theta). \tag{6}$$

We call $\Delta\mathrm{SF}_j$ the relation space, and the larger $\Delta\mathrm{SF}_j$ is, the more likely the optimal strategic direction is contained in it. However, if the areas of two SFSs are equal, it is impossible to find the optimal strategic direction by only comparing the areas. Both the area and the space angle of a SFS affect the selection of the optimal strategic direction. The larger the space angle, the wider the SFS. Therefore, an impact factor M is introduced and designated as the relation space factor, and it is written as

$$M_j = \Delta\mathrm{SF}_j \cdot \theta_j. \tag{7}$$

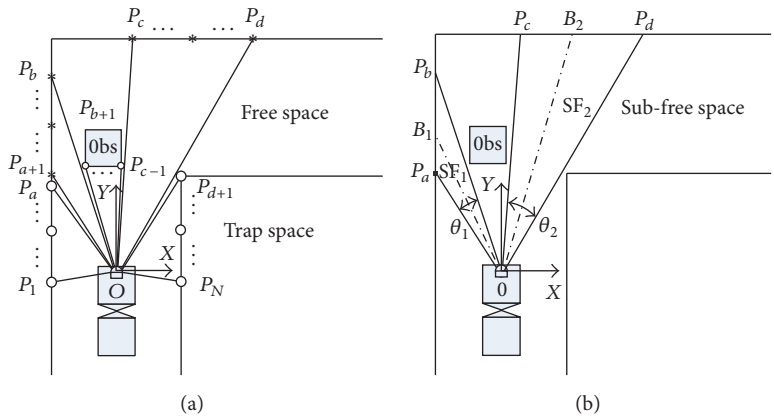

Figure 3: Free space and trap space ($a, b, c, d \in Z,\ 2 < a < b < c < d < N$).

The optimal strategic direction is $M_{\max}$, which can be obtained by

$$M_{\max} = \max\left\{M_1, M_2, \ldots, M_j\right\}. \tag{8}$$

3. Driving Control for an Articulated Vehicle

3.1. Kinematics Model of an Articulated Vehicle. Driving control for articulated vehicles includes steering and speed control. An underground mining vehicles' top speed is usually low (25 km/h) and its gross dead weight is very large; therefore, we assume that the wheels of the articulated vehicle do not slip. Figure 4 shows the geometry of an articulated vehicle in steering operations. The dynamic model of the articulated vehicle considered in this paper has a front section and rear section, which are connected by a joint H. The front and rear sections can rotate relative to each other, and steering is achieved by driving the articulation joint. In Figure 4, λ refers to the articulated angle and V refers to the ground speed of the front body; η_1 and η_2 are defined as the orientation angle of the front body and back body with respect to x-axis, respectively. The half-length of the body is defined as the distance between the front bumper or rear bumper of the vehicle and the articulation joint, referred to as l_1 and l_2, respectively. $P_1(x_1, y_1)$ and $P_2(x_2, y_2)$ refer to the coordinates of the middle point of the vehicle's front and rear bumpers, respectively. Point O'' is the center of the turning circle, and r_1 and r_2 are defined as the distance between O'' and P_1, P_2, respectively [19–23].

The equations of lines P_1H and P_2H are, respectively, defined as

$$y = k_1 \cdot x + b_1, \tag{9}$$

$$y = k_2 \cdot x + b_2, \tag{10}$$

where k_1 and b_1 are the linear slope and intercept of line P_1H, respectively, and k_2 and b_2 are the linear slope and intercept of line P_2H, respectively. Combining (9) and (10),

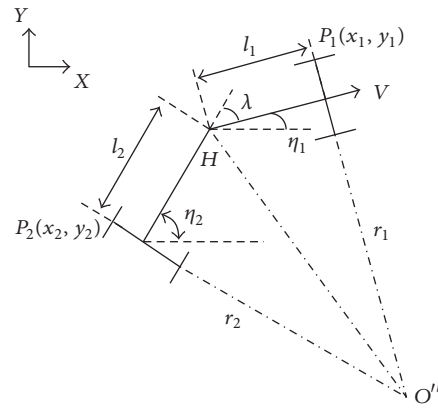

Figure 4: Geometry of the articulated vehicle while steering.

it is straightforward to obtain the coordinates of point O'' as follows:

$$x = \frac{b_2 - b_1}{k_1 - k_2},$$
$$y = k_1 \cdot \frac{b_2 - b_1}{k_1 - k_2} + b_1. \tag{11}$$

Based on the dynamic characteristics of the articulated vehicle, for the first body, we have

$$\dot{x_1} = v \cdot \cos\eta_1,$$
$$\dot{y_1} = v \cdot \sin\eta_1. \tag{12}$$

According to the geometric relationship of P_1 and P_2, we can show that

$$x_2 + l_2 \cdot \cos\eta_2 + l_1 \cdot \cos\eta_1 = x_1,$$
$$y_2 + l_2 \cdot \sin\eta_2 + l_1 \cdot \sin\eta_1 = y_1, \tag{13}$$

and it is straightforward to obtain

$$\eta_1 = \eta_2 - \gamma. \tag{14}$$

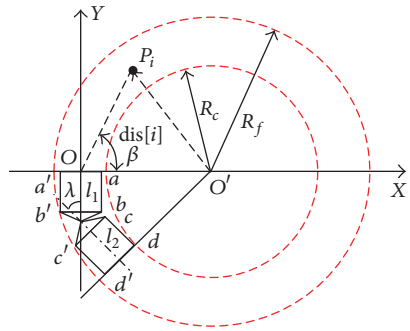

FIGURE 5: Obstacles along the vehicle's trajectory.

Since we have assumed that there is no slip, we have

$$\begin{aligned} \dot{x_2} \cdot \sin \eta_2 - \dot{y_2} \cdot \cos \eta_2 &= 0, \\ \dot{x_1} \cdot \sin \eta_1 - \dot{y_1} \cdot \cos \eta_1 &= 0. \end{aligned} \tag{15}$$

Differentiating (11) with respect to time, substituting in (12) and (15), the angular velocity equation is obtained as follows:

$$\dot{\eta_1} = \frac{-v \cdot \sin \gamma - l_2 \cdot \dot{\gamma}}{l_1 \cdot \cos \gamma + l_2}. \tag{16}$$

3.2. Obstacles along the Vehicle's Trajectory. It is important to determine the obstacles along the vehicle's trajectory, since they affect the vehicle's driving strategy. Figure 5 shows the obstacles along the trajectory, where O is the center of the laser radar and also the original point of the coordinate system; the points a, b, c, d and a', b', c', d' refer to the vehicle's edge points on the right-hand side and left-hand side, respectively. λ refers to the articulated angle, O' refers to the center point of the trajectory ring, P_i refers to the position of the obstacle, D_{OP_i} refers to the linear distance between O and P_i, and β refers to the orientation of line OP_i with respect to the x-axis. R_c and R_f are the inner and outer diameters of the trajectory ring, respectively, and l_1 and l_2 are the lengths of the front and rear parts of the trajectory ring, respectively.

Based on the geometric relationship, we have

$$\begin{aligned} x_i &= D_{OP_i} \cdot \cos \beta, \\ y_i &= D_{OP_i} \cdot \sin \beta. \end{aligned} \tag{17}$$

The coordinate of point O' can be written as

$$\begin{aligned} x_{O'} &= l_2 \cdot \sin \lambda + \frac{l_1 + l_2 \cdot \cos \lambda}{\tan \lambda}, \\ y_{O'} &= 0. \end{aligned} \tag{18}$$

It can be seen that when the vehicle turns right,

$$\begin{aligned} R_c &= \min \left(D_{O'a}, D_{O'd} \right), \\ R_f &= \max \left(D_{O'b'}, D_{O'c'} \right), \end{aligned} \tag{19}$$

where $D_{O'a}$, $D_{O'd}$, $D_{O'b'}$, and $D_{O'c'}$ refer to the distance between O' and a, d, b', and c', respectively, especially when $l_1 = l_2$, $D_{O'a} = D_{O'd}$, and $D_{O'b'} = D_{O'c'}$. The distance between P_i and O' is denoted as dis$[i]$ $(i = 1, 2, 3, \ldots, N)$:

$$\text{dis}\,[i] = \sqrt{\left(D_{OP_i} \cdot \cos \beta - \left(l_2 \cdot \sin \lambda + \frac{l_1 + l_2 \cdot \cos \lambda}{\tan \lambda} \right) \right)^2 + \left(D_{OP_i} \cdot \sin \beta \right)^2}. \tag{20}$$

The obstacles along the trajectory ring actually affect the vehicle's driving; these obstacles are designated as positive obstacles in this paper. These positive obstacles can be selected by the following equation:

$$R_c \le \text{dis}\,[i] \le R_f. \tag{21}$$

The coordinates of the positive obstacles are saved in array Q as

$$Q = \left\{ (x_1, y_1), (x_2, y_2), (x_3, y_3), \ldots, (x_i, y_i) \right\}. \tag{22}$$

3.3. Data-Based Steering and Speed Control Module. The trajectory of the articulated vehicle and the obstacles affecting the vehicle's driving have been analyzed in the preceding sections. The steering and speed control are very important parts of the vehicle's overall driving control, the effects of which mostly depend on the vehicle's kinematics model [24, 25]. Therefore, it is essential to build the vehicle's steering and speed kinematics models as accurately as possible, a strategy validated by the fact that a data-driven approach to control methodology has improved the navigational efficiency of ground robots [26, 27]. For the method described in this paper, the steering and speed models are built based on the vehicle's operation data in order to reduce the modeling complexity.

3.3.1. Data-Based Steering Control Module. It is easy to collect the vehicle's articulated angle, steering time, and so forth, which can clearly reflect the vehicle's steering kinematics model. The optimal strategic direction has been found using the RSM. The articulated angle is denoted as λ and the angle of optimal strategic direction with respect to the x-axis in the coordinate system is denoted as φ, with each φ relative to an articulated angle $\lambda_{(\text{strategy})}$. It is known that each articulated angle is relative to a time point; therefore, the steering time $T_{S(L\text{-}R)}$ (steering from left to right) or $T_{S(R\text{-}L)}$ (steering from right to left) from a given current position to a strategic direction can be obtained using the dichotomy principle. In consideration of driving smoothness and safety, a threshold

value, denoted as T_S, is set. T_S is an experience parameter that can prevent the vehicle from steering too often. The steering rules are as follows:

(i) If $\lambda - \lambda_{(\text{strategy})} > 0$ and $T_{S(R\text{-}L)} \le T_S$, then steer left.

(ii) If $\lambda - \lambda_{(\text{strategy})} < 0$ and $T_{S(L\text{-}R)} \le T_S$, then steer right.

(iii) $T_{S(L\text{-}R)} > T_S$ and $T_{S(R\text{-}L)} > T_S$; then maintain the current articulated angle.

These rules not only make the vehicle drive along the strategic direction but also improve its driving smoothness.

3.3.2. Data-Based Speed Control Module. Unlike passenger vehicles, the articulated mining vehicles' driving mode is much simpler, typically consisting of constant, acceleration, deceleration, and braking modes. It is easy to collect the vehicle's driving speed and time, which can clearly reflect the vehicle's speed kinematics model.

The effects of positive obstacles on the vehicle's speed control have been analyzed previously. To ensure the safety of articulated vehicles, allowance δ' is introduced in the speed control. The trajectory for speed control can be rewritten as

$$R_c - \delta' \le \text{dis}\,[i] \le R_f + \delta', \tag{23}$$

in which allowance δ' acts as an experience parameter that can offset speed control errors. Based on (23), the objective obstacle points in the speed control are obtained, which are saved in array Q_V:

$$\begin{aligned} &Q_V \\ &= \left\{\left(x_{V_1}, y_{V_1}\right), \left(x_{V_2}, y_{V_2}\right), \left(x_{V_3}, y_{V_3}\right), \ldots, \left(x_{V_i}, y_{V_i}\right)\right\}. \end{aligned} \tag{24}$$

The distance between the vehicle and the obstacles in Q_V is actually arcs, denoted as D_{V_i}; therefore, we have

$$\begin{aligned} D_{V_i} &= \arcsin \frac{\left|y_{V_i}\right|}{\sqrt{{y_{V_i}}^2 + \left(x_{V_1} - x_{V_i}\right)^2}} \cdot \text{dist}\,[i] \\ &\qquad (1 \le i \le N), \end{aligned} \tag{25}$$

and the minimum value of D_{V_i} is

$$D_{V\min} = \min\left\{D_{V_1}, D_{V_2}, D_{V_3}, \ldots, D_{V_i}\right\}. \tag{26}$$

The vehicle's driving time considering $D_{V\min}$ at a speed v can be written as

$$T = \frac{D_{V\min}}{v}. \tag{27}$$

It can be seen from (25)–(27) that each velocity is relative to a time point, and therefore the driving times considering $D_{V\min}$ in deceleration and braking modes are denoted as T_d and T_b, respectively.

The drivers can change the vehicle's driving mode by comparing T, T_d, and T_b. In the method described in this paper, the vehicle's speed control is achieved by imitating the driver's driving habits, and the control rules are as follows:

(i) If $T > k_d \cdot T_d$, then speed up.

(ii) If $T_d < T \le k_d \cdot T_d$, then maintain current speed.

(iii) If $k_b T_b < T \le T_d$, then slow down.

(iv) If $T \le k_b \cdot T_b$, then brake.

In the above rules, k_b and k_d are amplification factors for braking and deceleration times, respectively ($0 < k_b < 1$, $k_d > 1$). These amplification factors provide allowance for not only eliminating errors but also ensuring the safety of the vehicle; they can be adjusted according to the sizes of the vehicle and of the tunnel. The amplification factors and safety distance, denoted as L, are indispensable. The vehicle will initiate emergency braking immediately if the distance between the vehicle and the obstacles is shorter than L, which is the highest priority. The safety distance is related to the vehicle's structure, and it can further increase the vehicle's security; and $L = 15$ cm in this paper.

4. Simulation and Experiment

The original data of the vehicle's kinematics model are collected from the articulated vehicle prototype and include speed, articulated angle, and time. Two steering and three speed kinematics models of an articulated vehicle are generated using these data. In this paper, the order of the steering and speed fitting equations is 3. Figure 6 shows the fitting curves of the vehicle steering process. The black asterisks represent the original data, the blue line represents the fitting curve, and the red line indicates the fitting error. The two steering kinematics models include steering from left to right and steering from right to left.

The cubic fitting equations of steering from left to right and steering from right to left are written, respectively, as

$$\begin{aligned} \lambda_{L\text{-}R} &= 0.0538t^3 - 1.4437t^2 + 15.9857t - 50.9267 \\ &\qquad (0 \le t \le 13.6), \\ \lambda_{R\text{-}L} &= -0.0376t^3 + 1.0408t^2 - 14.8118t - 48.1576 \\ &\qquad (0 \le t \le 12.6). \end{aligned} \tag{28}$$

Figure 7 shows the vehicle speed fitting curves in different driving modes. The three speed kinematics modes include acceleration, deceleration, and braking.

The cubic fitting equations of the vehicle acceleration, deceleration, and braking modes can be written, respectively, as

$$\begin{aligned} V_a &= 0.039528t^3 - 0.435515t^2 + 1.645189t \\ &\quad - 0.0913833 \quad (0 \le t \le 4.8), \\ V_d &= 0.004281t^3 - 0.077942t^2 + 0.149005t \\ &\quad + 2.0259928 \quad (0 \le t \le 9.7), \\ V_b &= -24.309795t^3 - 56.591949t^2 - 32.670702t \\ &\quad + 2.232053 \quad (0 \le t \le 1.4). \end{aligned} \tag{29}$$

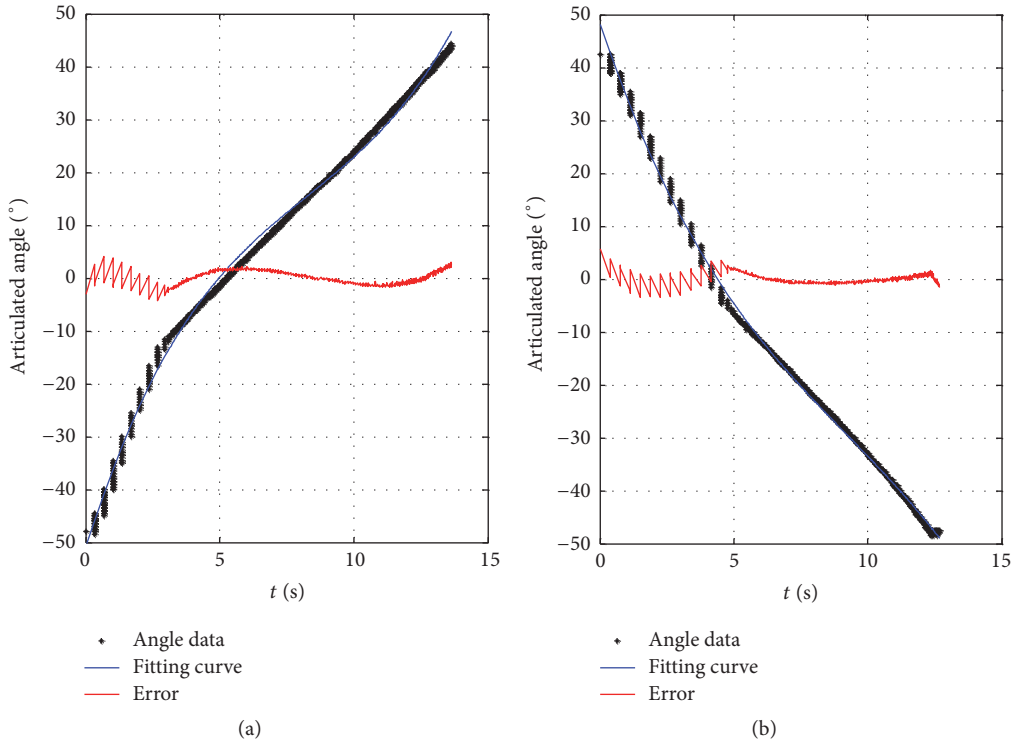

Figure 6: Fitting curves for the vehicle steering from (a) left to right and from (b) right to left.

4.1. Simulation. We have developed software, the interface of which is shown in Figure 8, to simulate an articulated vehicle driving in a tunnel environment. The articulated vehicle kinematics models were built before running the simulation. The structure parameters of the articulated vehicle and tunnel can be reset in the software, which were initially set according to an articulated vehicle prototype in our lab and the corridor of our laboratory building.

Figure 9 shows the driving tracks of the articulated vehicle based on the RSM in different tunnels. In the tunnel depicted in Figure 9(a), there is one sharp curve and one intersection; in that depicted in Figure 9(b), there is one right-angle curve and several obtuse-angle curves. The simulation result shows that the vehicle can drive in different tunnels smoothly.

4.2. Experiment

4.2.1. Articulated Vehicle Prototype. After the algorithms have been verified in the simulation environment, we conducted experiments on our autonomous prototype research platform to verify the proposed control strategy. Figure 10(a) is a structural diagram of the prototype, while Figure 10(b) is a photograph of the prototype in our laboratory. The prototype is scaled down based on a real mining vehicle, which includes one SICK LMS511-10100 laser radar, one ADVANTEC ARK-3500 (Intel i5, 2.5 GHz processor) industrial personal computer (IPC), one EPEC (3724) programmable logic controller, two DSP (TMS320F2808) drivers, one steering motor, one angle encoder, and one remote controller. The laser radar is mounted in the front body, with a detection range of 80 m and a detection angle range of −5° to 185° from left to right in steps of 1°, including 190 detection points. The update frequency of the data detection is 100 Hz. The IPC is physically the upper computer depicted in the figure used to identify the space information and run the relation space algorithm, while the EPEC is the lower computer. Two DSP drivers are used to drive the brushless direct current (BLDC) motors. The angle encoder is used to detect the articulated angle of the prototype.

Table 1: Characteristics of articulated vehicle prototype.

Spec.	Value
Length of front body	521.5 mm
Length of rear body	528.2 mm
Width	1049.7 mm
Tire radius	201.5 mm
Rotation range	Right, 47.9°; left, 44.4°
Top speed	2.14 m/s

Table 1 lists the characteristics of the prototype.

Figure 11 shows the map of the laboratory corridor in which the experiments were conducted. The width of the corridor is 2.2 m and the driving distance in the experiment is 40 m, starting from point A and stopping at D. The width ratio of the prototype to the corridor is very close to reality.

4.2.2. Experimental Results. We chose positions A, B, and C for space identification using a self-organizing, competitive neural network. Position A is the general tunnel, position B

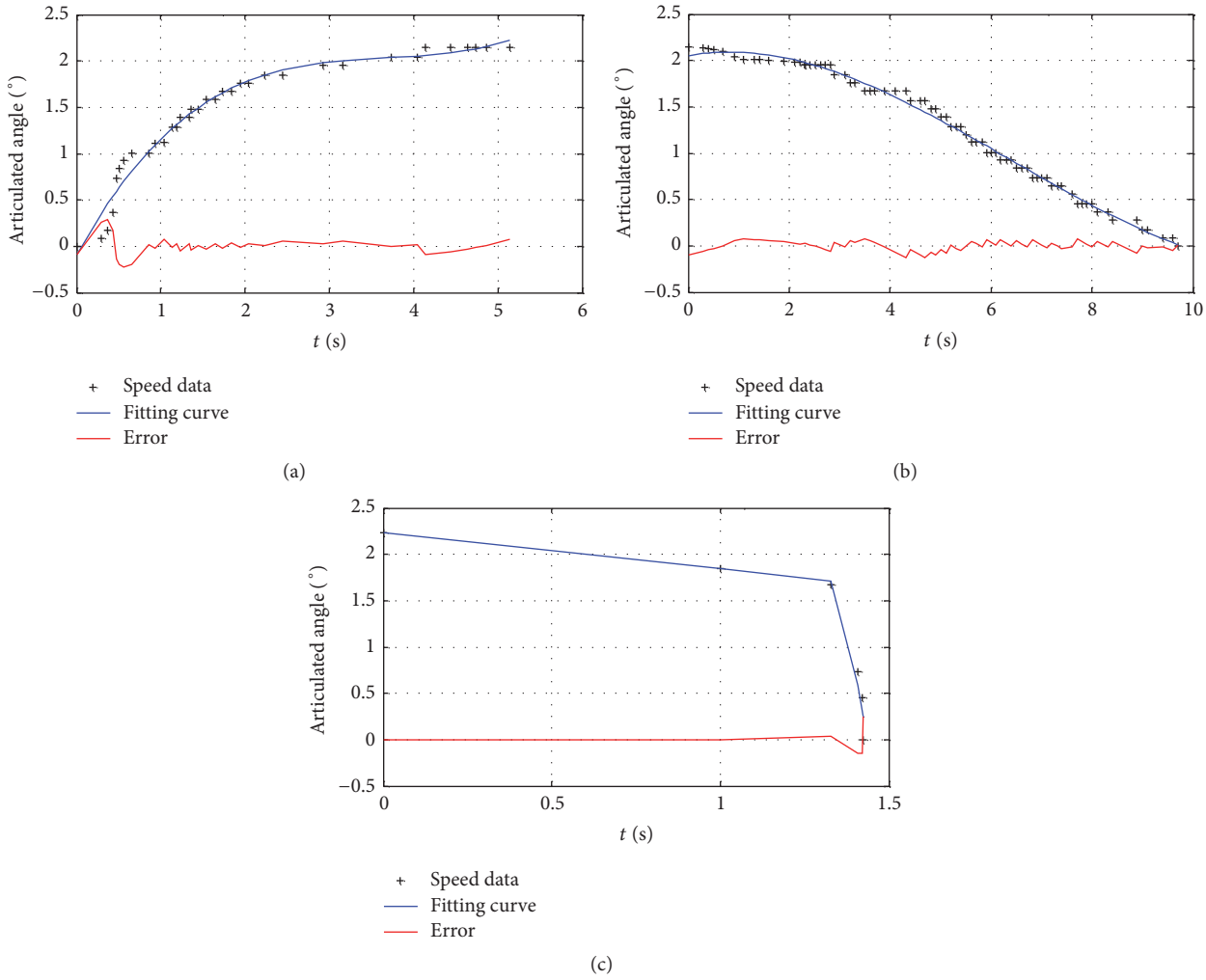

Figure 7: Fitting curves of different speed modes: (a) acceleration; (b) deceleration; and (c) braking.

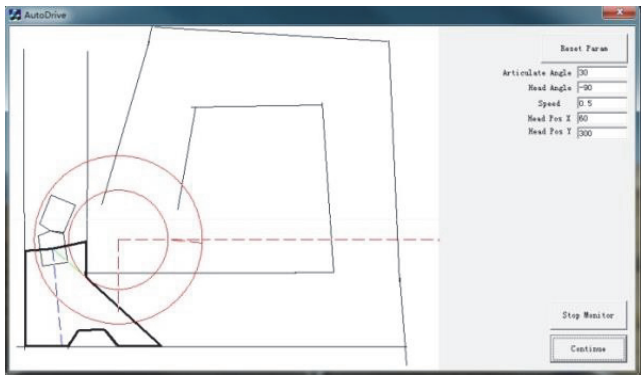

Figure 8: Simulation software interface.

is the cross-road tunnel, and position C is the bend tunnel. We tested the space identification twice at C, once with no obstacles in the corner and once with an obstacle set up in the corner. The experiments essentially covered all navigational situations that an articulated vehicle may encounter driving in underground mining tunnels. Figure 12 shows the result of space identification; the blue asterisks represent the free space, the red open circles represent the trap space, and the five-pointed stars represent the normalized center of the self-organizing, competitive neural network. It can be seen in the figure that the space can be classified into free space and trap space effectively in various driving situations using a self-organizing, artificial neural network.

We also performed multigroup driving experiments in auto and manual modes, respectively. The space identification and driving control methods proposed in this paper are applied in auto mode. The most skilled person drives the prototype by remote controller in manual mode. Figure 13 shows the vehicle's articulated angle and speed during this experiment. The blue lines represent manual mode and the red lines represent auto mode. Specifically, Figure 13(a) shows that the articulated angle varies with time in both auto and manual modes, with right turns marked with a positive number and left turns marked with a negative number. It can be seen in the figure that the articulated angle has little fluctuation in auto mode. In the course of turning the corner,

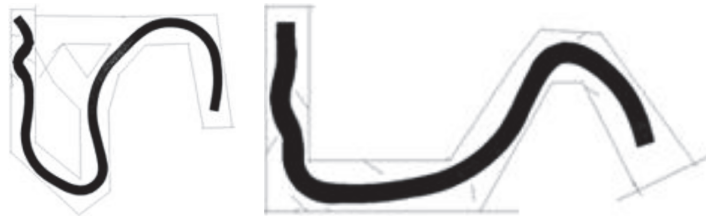

(a) (b)

Figure 9: Simulation results of the articulated vehicle driving in different tunnels.

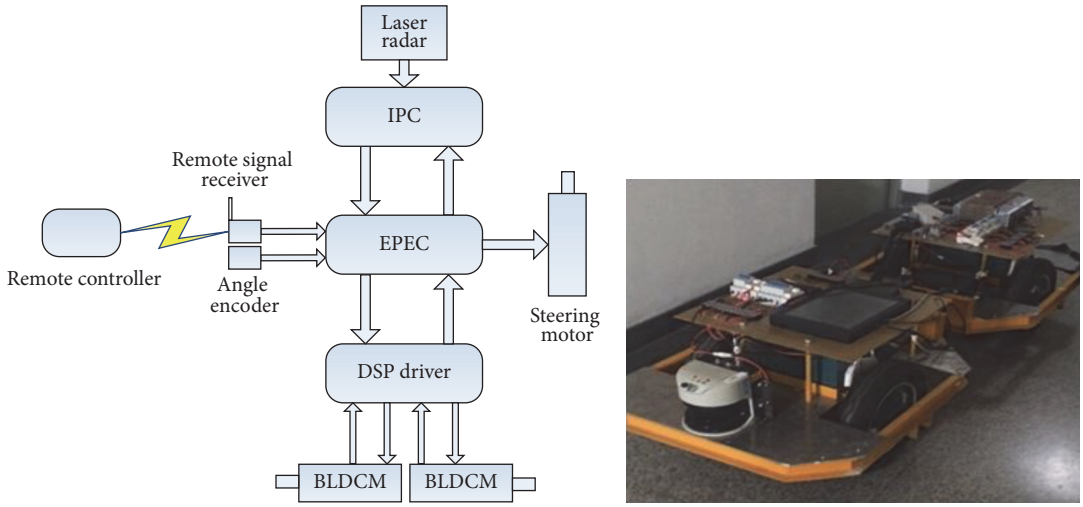

(a) (b)

Figure 10: Articulated vehicle prototype.

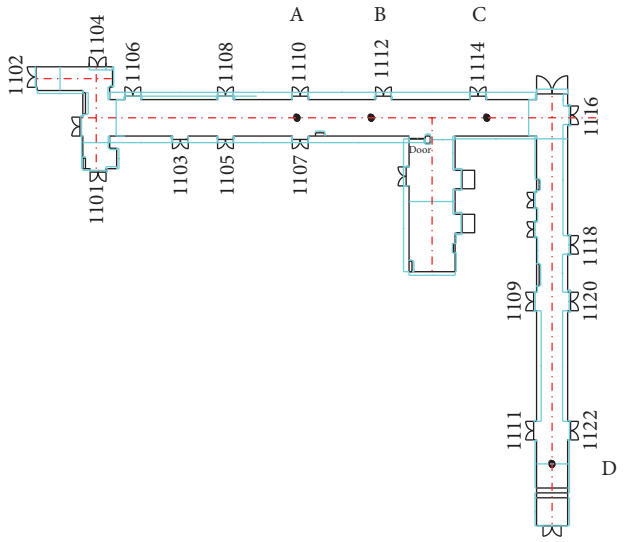

Figure 11: Map of corridor.

the articulated angle changes from left 11° to right 47° in manual mode, while it changes from left 10° to right 40° in auto mode. The smaller fluctuation of the articulated angle could make the prototype drive more smoothly and more stably. Figure 13(b) shows that the velocity varies with time in both auto and manual modes. It can be seen that the maximum speed in both modes is approximately 2 m/s; however, the average speeds are 0.8 and 0.75 m/s in auto and manual modes, respectively. These results prove that the relative navigation method proposed in this paper is efficient.

5. Conclusions

This paper reports the results of an investigation of a relative navigation strategy based on the relation space method (RSM) for autonomous underground articulated vehicles. In the RSM, a self-organizing neural network was used to identify the vehicle's driving space, and the vehicle's optimal driving direction was determined using the spatial geometric relationships of the identified space, which allowed us to automatically obtain the correct direction to drive in various kinds of tunnels. The kinematics model of the articulated structure was deeply analyzed and applied to the speed and steering control of the vehicle. In order to reduce modeling complexity and improve computational efficiency, straightforward steering and speed control modules were built on the basis of the vehicle's operation data, which is straightforward to implement in different vehicles even without knowing the

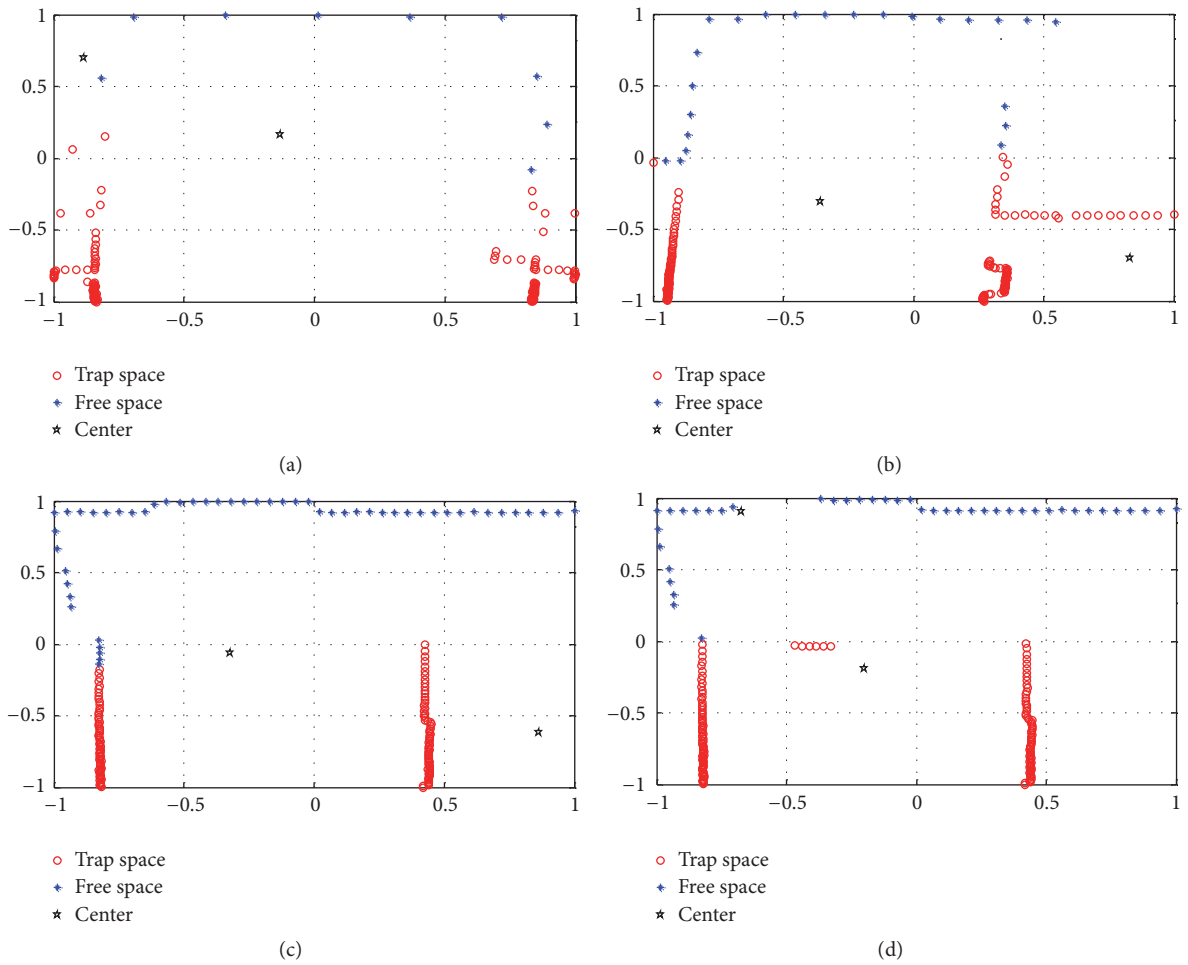

FIGURE 12: Result of space identification at (a) position A, (b) position B, (c) position C without a barrier in the corner, and (d) position C with an obstacle in the corner.

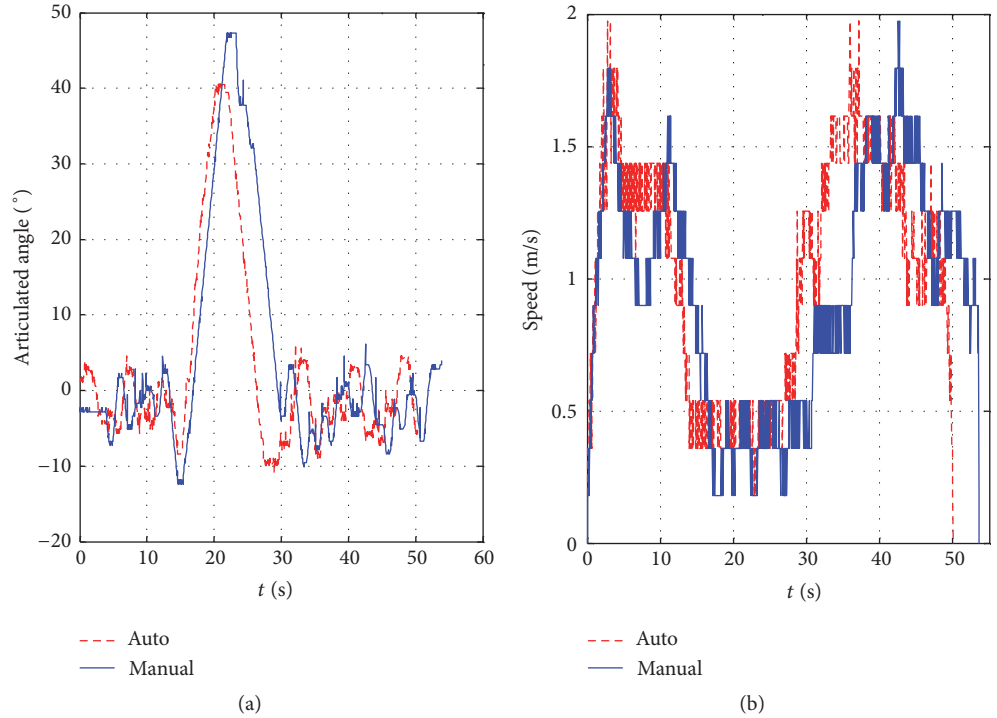

FIGURE 13: Driving experiment results.

specific vehicle parameters. Software was developed to verify the feasibility of primarily the driving control method. An additional set of experiments were carried out in the corridor of our laboratory using an articulated vehicle prototype. One set of experiments featured driving the prototype in manual mode by a driver with a remote controller; the other set used the automated driving method proposed in this paper. The results show that the vehicle can choose the correct direction over the course of the entire journey by applying the new method. Moreover, the articulated angle of the prototype in auto mode is less volatile than the articulated angle in manual mode, and, moreover, the average speed is improved. Comparisons of the results demonstrate the feasibility and effectiveness of the new strategy.

Competing Interests

The authors declare that they have no competing interests.

Acknowledgments

This work was supported by a grant from the National High Technology Research and Development Program of China (no. 2011AA060408), Beijing Higher Education Young Elite Teacher Project (no. YETP0362), and Fundamental Research Funds for the Central Universities (no. FRF-TP-14-024A2 and no. FRF-TP-15-023A1).

References

[1] N. Vagenas, M. Scoble, and G. Baiden, "A review of the first 25 years of machine automation in underground hard rock mines," *CIA4 Bulletin*, vol. 1006, no. 90, pp. 57–62, 1997.

[2] D. Akopian and J. Syrjarinne, "A fast positioning method without navigation data decoding for assisted GPS receivers," *IEEE Transactions on Vehicular Technology*, vol. 58, no. 8, pp. 4640–4645, 2009.

[3] H. Nonaka and T. Da-Te, "Ultrasonic position measurement and its applications to human interface," *IEEE Transactions on Instrumentation and Measurement*, vol. 44, no. 3, pp. 771–774, 1995.

[4] J.-H. Wang and Y. Gao, "Land vehicle dynamics-aided inertial navigation," *IEEE Transactions on Aerospace and Electronic Systems*, vol. 46, no. 4, pp. 1638–1653, 2010.

[5] S. A. Hiremath, G. W. A. M. van der Heijden, F. K. van Evert, A. Stein, and C. J. F. ter Braak, "Laser range finder model for autonomous navigation of a robot in a maize field using a particle filter," *Computers and Electronics in Agriculture*, vol. 100, pp. 41–50, 2014.

[6] J. M. Roberts, "Autonomous control of underground mining vehicles using reactive navigation," in *Proceedings of the IEEE International Conference on Robotics and Automation (ICRA '00)*, San Francisco, Calif, USA, April 2000.

[7] M. Lepetič, G. Klančar, I. Škrjanc, D. Matko, and B. Potočnik, "Time optimal path planning considering acceleration limits," *Robotics and Autonomous Systems*, vol. 45, no. 3-4, pp. 199–210, 2003.

[8] X. Li, Z. Sun, D. Cao, D. Liu, and H. He, "Development of a new integrated local trajectory planning and tracking control framework for autonomous ground vehicles," *Mechanical Systems and Signal Processing*, 2015.

[9] R.-E. Precup, E. M. Petriu, L.-O. Fedorovici, M.-B. Radac, and F. Dragan, "Multi-robot charged system search-based optimal path planning in static environments," in *Proceedings of the IEEE International Symposium on Intelligent Control (ISIC '14)*, pp. 1912–1917, October 2014.

[10] H. Ishimoto, T. Tsubouchi, S. Sarata, and S. Yuta, "A practical trajectory following of an articulated steering type vehicle," in *Field and Service Robotics*, A. Zelinsky, Ed., pp. 397–404, 1998.

[11] A. Hemamiand and V. Polotski, "Path tracking control problem for mulation of an LHD loader," *The International Journal of Robotics Research*, no. 17, pp. 193–199, 1998.

[12] J. D. Lane, *Automatic steering system for an underground mine haul truck [M.S. thesis]*, Colorado School of Mines, 1992.

[13] J. D. Lane, *Automatic steering system for an underground mine haul truck [M.S. thesis]*, Colorado School of Mines, Golden, Colo, USA, 1992.

[14] J. P. H. Steele, R. King, and W. Strickland, "Modeling and sensor-based control of an autonomous mining machine," in *Proceedings of the 4th International Symposium on Mine Mechanisation and Automation*, pp. 6.55–6.67, Golden, Colo, USA, June 1991.

[15] T. M. Ruff, "Ultrasonic guidance and remote control of a compact loader/trammer," in *Proceedings of the International Symposium on Mine Mechanisation and Automation*, pp. 6.45–6.54, Golden, Colo, USA, June 1991.

[16] J. M. Roberts, E. S. Duff, and P. I. Corke, "Reactive navigation and opportunistic localization for autonomous underground mining vehicles," *Information Sciences*, vol. 145, no. 1-2, pp. 127–146, 2002.

[17] R. Guo-Feng and T. Zhu-Mei, "Application of self-organizing competitive network in lithologic identification of the logging data," in *Proceedings of the International Conference on Computing, Measurement, Control and Sensor Network*, pp. 148–151, 2012.

[18] X. Wang, A. Liu, Y. Sun, Y. Wang, Y. Han, and H. Wang, "Evaluation method of beef tenderness based on texture properties and self-organizing neural network model," *Transactions of the Chinese Society of Agricultural Engineering*, vol. 31, no. 18, pp. 262–268, 2015.

[19] S. Scheding and G. Dissanayake, "An experiment in autonomous navigation of an underground mining vehicle," *IEEE Transactions on Robotics and Automation*, vol. 15, no. 1, pp. 85–95, 1999.

[20] P. I. Corke and P. Ridley, "Steering kinematics for a center-articulated mobile robot," *IEEE Transactions on Robotics and Automation*, vol. 17, no. 2, pp. 215–218, 2001.

[21] D. Chwa, "Sliding-mode tracking control of nonholonomic wheeled mobile robots in polar coordinates," *IEEE Transactions on Control Systems Technology*, vol. 12, no. 4, pp. 637–644, 2004.

[22] I. Baturone, F. J. Moreno-Velo, V. Blanco, and J. Ferruz, "Design of embedded DSP-Based fuzzy controllers for autonomous mobile robots," *IEEE Transactions on Industrial Electronics*, vol. 55, no. 2, pp. 928–936, 2008.

[23] D. Chwa, "Tracking control of differential-drive wheeled mobile robots using a backstepping-like feedback linearization," *IEEE Transactions on Systems, Man, and Cybernetics Part A: Systems and Humans*, vol. 40, no. 6, pp. 1285–1295, 2010.

[24] P. Rusu, E. M. Petriu, T. E. Whalen, A. Cornell, and H. J. W. Spoelder, "Behavior-based neuro-fuzzy controller for mobile robot navigation," *IEEE Transactions on Instrumentation and Measurement*, vol. 52, no. 4, pp. 1335–1340, 2003.

[25] C.-H. Hsu and C.-F. Juang, "Evolutionary robot wall-following control using type-2 fuzzy controller with species-DE-activated continuous ACO," *IEEE Transactions on Fuzzy Systems*, vol. 21, no. 1, pp. 100–112, 2013.

[26] C.-F. Juang, Y.-H. Chen, and Y.-H. Jhan, "Wall-following control of a hexapod robot using a data-driven fuzzy controller learned through differential evolution," *IEEE Transactions on Industrial Electronics*, vol. 62, no. 1, pp. 611–619, 2015.

[27] M. Al-Khatib and J. J. Saade, "An efficient data-driven fuzzy approach to the motion planning problem of a mobile robot," *Fuzzy Sets and Systems*, vol. 134, no. 1, pp. 65–82, 2003.